

UV SURFACE ENVIRONMENT OF EARTH-LIKE PLANETS ORBITING FGKM STARS THROUGH GEOLOGICAL EVOLUTION

S. RUGHEIMER^{1,3}, A. SEGURA², L. KALTENEGGER³, AND D. SASSELOV¹

¹ Harvard Smithsonian Center for Astrophysics, 60 Garden st., 02138 MA Cambridge, USA; srugheimer@cfa.harvard.edu

² Instituto de Ciencias Nucleares, Universidad Nacional Autónoma de México, México

³ Carl Sagan Institute, Cornell University, Ithaca, NY 14853 USA

Received 2014 October 27; accepted 2015 May 1; published 2015 June 12

ABSTRACT

The UV environment of a host star affects the photochemistry in the atmosphere, and ultimately the surface UV environment for terrestrial planets and therefore the conditions for the origin and evolution of life. We model the surface UV radiation environment for Earth-sized planets orbiting FGKM stars in the circumstellar Habitable Zone for Earth through its geological evolution. We explore four different types of atmospheres corresponding to an early-Earth atmosphere at 3.9 Gyr ago and three atmospheres covering the rise of oxygen to present-day levels at 2.0 Gyr ago, 0.8 Gyr ago, and modern Earth. In addition to calculating the UV flux on the surface of the planet, we model the biologically effective irradiance, using DNA damage as a proxy for biological damage. We find that a pre-biotic Earth (3.9 Gyr ago) orbiting an F0V star receives 6 times the biologically effective radiation as around the early Sun and 3520 times the modern Earth–Sun levels. A pre-biotic Earth orbiting GJ 581 (M3.5 V) receives 300 times less biologically effective radiation, about 2 times modern Earth–Sun levels. The UV fluxes calculated here provide a grid of model UV environments during the evolution of an Earth-like planet orbiting a range of stars. These models can be used as inputs into photo-biological experiments and for pre-biotic chemistry and early life evolution experiments.

Key words: astrobiology – Earth – planets and satellites: surfaces – planets and satellites: terrestrial planets

1. INTRODUCTION

Thousands of extrasolar planets have been found to date with thousands more awaiting confirmation from space and ground-based searches. Several of these planets have been found in or near the circumstellar Habitable Zone (see, e.g., Udry et al. 2007; Borucki et al. 2011, 2013; Kaltenegger & Sasselov 2011; Batalha et al. 2013; Kaltenegger et al. 2013; Quintana et al. 2014) with masses and radii consistent with rocky planet models. The quest for finding habitable planets focuses on main-sequence stars with lifetimes conducive for the origin and evolution of life, namely, the F, G, K, and M spectral types with stellar main-sequence lifetimes at least 2 Gyr or more. The UV environment of a host star will affect the atmosphere, and ultimately the surface UV environment for terrestrial planets. (see e.g., Segura et al. 2003; Rugheimer et al. 2013, 2014; Sato et al. 2014).

Future mission concepts to characterize Earth-like planets are designed to take spectra of extrasolar planets with the ultimate goal of remotely detecting atmospheric signatures that can indicate habitability and life (e.g., Beichman et al. 1999, 2006; Cash 2006; Kaltenegger et al. 2006; Traub et al. 2006; Seager & Bains 2015). The UV surface environment for planets is an important component in providing boundary conditions for biological models exploring the origin of life on Earth as well as planets orbiting other types of stars.

Depending on the intensity, UV radiation can be both useful and harmful to life as we know it. UV radiation from 180–300 nm can inhibit photosynthesis and cause damage to DNA and other macromolecule damage (Voet et al. 1963; Matsunaga et al. 1991; Tevini 1993; Kerwin & Remmele 2007). However, these same wavelengths also drive several reactions thought necessary for the origin of life (e.g., Senanayake & Idriss 2006; Barks et al. 2010; Ritson & Sutherland 2012; Patel et al. 2015). In this paper we model the

UV surface radiation environments for both pre-biotic and post-biotic planets orbiting other stars at the 1 AU equivalent distance based on Earth’s evolution.

Previous studies used an analytic atmospheric attenuation model to model UV environment for Archean Earth (Cockell 1998, 1999, 2000; Cnossen et al. 2007) as well as F stars (Sato et al. 2014). An earlier study (Segura et al. 2003) examined the amount of UV radiation reaching the surface of an Earth-like planet with varying oxygen atmospheric concentration orbiting an F2V, G2V (the Sun), and K2V host star. Our paper expands the grid of host stars as well as models of the UV surface environments for atmospheres that correspond to geological epochs throughout Earth’s evolution (following Kaltenegger et al. 2007). We focus on four geological epochs corresponding to a 3.9 Ga (assumed prebiotic)⁴, 2.0 Ga, 0.8 Ga, and the modern Earth atmosphere for a grid of FGKM host stars.

In Section 2, we describe our model, Section 3 presents the calculated UV fluxes at the surface and top of the atmosphere of an Earth-like planet for 12 stellar types and the four different atmosphere models through geological time. In Section 4 we conclude by summarizing the results and discussing their implications.

2. MODEL DESCRIPTION

2.1. Stellar and Planetary Model

We use a grid of host stars from F0V to M8V ($T_{\text{eff}} = 7000$ to 2400 K; see Rugheimer et al. 2013, 2014). All stellar models use observations in the UV by the *IUE*⁵ except for 3 M dwarfs with *Hubble Space Telescope HST* data and reconstructed Ly α fluxes (France et al. 2013) up to 3000 Å combined with

⁴ Ga—billion years ago.

⁵ <http://archive.stsci.edu/iue>

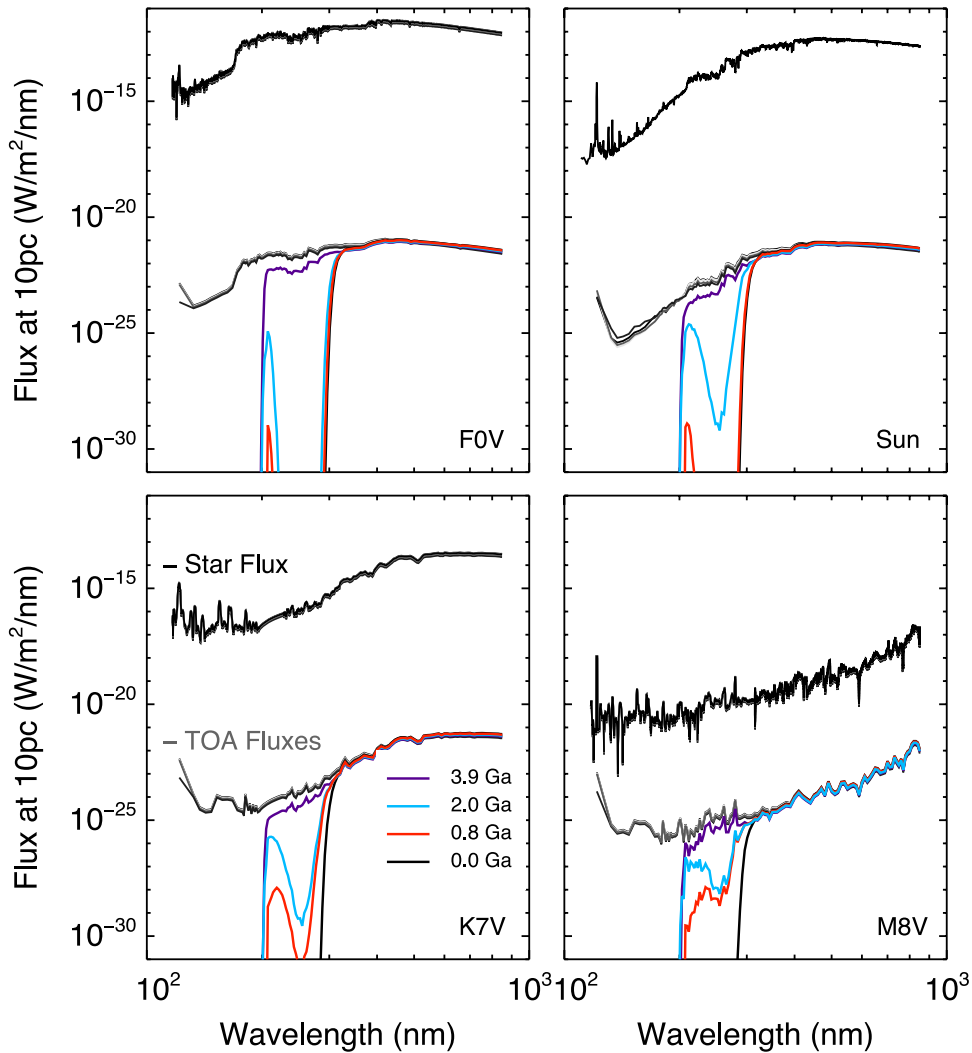


Figure 1. Stellar flux (black lines), TOA fluxes (gray lines), and surface UV fluxes (colored lines) for each of the four geological epochs for an F0V (top left), the Sun (top right), a K7V (bottom left), and M8V (bottom right) host star.

PHOENIX (Allard et al. 2000; Allard 2014) or ATLAS (Kurucz 1979) stellar models⁶ for larger wavelengths (F0V, F7V, Sun (G2V), G8V, K2V, K7V, M1V, M3V, M8V⁷). The three M dwarfs with updated UV data are GJ 581 (M3V, $T_{\text{eff}} = 3498$ K), GJ 832 (M1.5 V, $T_{\text{eff}} = 3620$ K), and GJ 1214 (M4.5 V, $T_{\text{eff}} = 3250$ K; France et al. 2013).

To model the planetary atmospheres, we use a coupled 1D radiative-convective atmosphere code developed for rocky exoplanets. It iterates between a 1D climate (Kasting & Ackerman 1986; Pavlov et al. 2000; Haqq-Misra et al. 2008) and a 1D photochemistry code (Pavlov & Kasting 2002; Segura et al. 2005, 2007) to calculate the atmosphere transmission of UV fluxes to the ground of Earth-sized planets.

We simulate the effects of stellar radiation on a planetary environment with an altitude range that extends upwards to 60 km, corresponding to a pressure of 1mbar, with 100 height layers. A two-stream approximation (see Toon et al. 1989), which includes multiple scattering by atmospheric gases, is

⁶ BT-Settl PHOENIX models are used for the M stars and ATLAS models are used for the FGK stars.

⁷ The M1V, M3V, and M8V are the active stellar models defined in Rugheimer et al. (2014).

used in the visible/near-IR to calculate the shortwave fluxes. Four-term, correlated- k coefficients parameterize the absorption by O_3 , H_2O , O_2 , and CH_4 (Pavlov et al. 2000). Clouds are not explicitly calculated. Clouds can either reduce or enhance UV radiation reaching the surface of an Earth-like planet (Grant & Heisler 1997; Parisi & Downs 2004). The climatic effects of clouds on the temperature versus pressure profile are included by adjusting the planet’s surface albedo to the value that for the modern Earth–Sun system yields a surface temperature of 288 K (following Kasting et al. 1984; Pavlov et al. 2000; Segura et al. 2003, 2005). The photochemistry code, originally developed by Kasting et al. (1985), solves for 55 chemical species linked by 220 reactions using a reverse-Euler method (see Segura et al. 2010, and references therein).

For the geological epoch at 3.9 Ga, we use a 1D photochemical model for high- CO_2 /high- CH_4 terrestrial atmospheres (see Pavlov et al. 2001; Kharecha et al. 2005; Segura et al. 2007, and references therein). This model simulates an anoxic atmosphere composed of 0.9 bar of N_2 and fixed amounts of CO_2 and CH_4 . We run the radiative-convective model to convergence and then use the resulting temperature profile to run the photochemical model that contains 73 chemical species involved in 359 reactions. The model spans

the region from the planetary surface up to 64 km in 1 km steps. All of the simulated planets at 3.9 Ga are assumed to be devoid of life; hence, none of the compounds in the atmosphere are considered to have a biological source.

2.2. Simulation Set-up

We focus on four geological epochs from Earth’s history to model the UV environment on the surface of an Earth-like planet at the 1 AU equivalent distance from its host star. The geological evidence from 2.8–3.5 Ga is consistent with an atmosphere with similar atmospheric pressure as modern Earth (Som et al. 2012; Marty et al. 2013). Therefore, we use one bar for the surface pressure for all epochs.

Currently no model can predict the rate of the evolution of life on planets around different stars which themselves have a different main sequence lifetimes. For the Earth–Sun case, we use a solar evolution model for each epoch (Claire et al. 2012). We reduce the stellar flux of all other host stars by the same factor as a first order approximation of how much stellar flux would be received at a corresponding epoch for the other host stars. This procedure is not meant to capture the nuances of stellar evolution. Rather, it is intended to compare across different stellar hosts for planets that receive the same bolometric flux with different atmospheric compositions modeled after Earth’s evolution. This translates into different evolutionary stages of the star–planet system as well as into different distances from the the host stars corresponding to 1.15–1 AU (75%–100% current insolation). Especially for M stars, which evolve much more slowly on the main sequence, reducing the stellar flux by the same amount as Earth is equivalent to increasing its distance from the host star. We model each of the four atmospheres for planets orbiting stars with spectral types of F0V, F7V, the Sun (G2V), G8V, K2V, K7V, M1V, M3V, and M8V to sample the FGKM spectral range along with three observed MUSCLES stars, GJ 581, GJ 832, and GJ 1214, with well characterized UV observations from *HST*.

The first epoch corresponds to a pre-biotic world, similar to early Earth at 3.9 Ga with a CO₂ dominated atmosphere. We model the atmosphere with a fixed surface mixing ratio of CO₂ = 0.1 and CH₄ = 1.65 × 10⁻⁶ and no biological gas fluxes. We assume a stellar flux of 74.6% of the present day Earth–Sun system.

The next three epochs represent planets with an active biosphere with oxygenic photosynthesis. To model atmospheres corresponding to a similar stage of biological evolution as Earth’s, we use calculated biological surface fluxes from the Earth–Sun model as inputs for the same epoch for all other stellar types as detailed in the following three paragraphs.

The second epoch corresponds to 2.0 Ga, when oxygen starts to build up in Earth’s atmosphere. We model the atmosphere with a fixed surface mixing ratio of CO₂ = 0.01 and O₂ = 2.1 × 10⁻³ (1% PAL = Present Atmospheric Level) and a stellar flux of 87%. For the Earth–Sun case we fix the mixing ratios of the other biological gases to CH₄ = 7.07 × 10⁻³ (4300x PAL), N₂O = 8.37 × 10⁻⁹, and CH₃Cl = 5.0 × 10⁻¹⁰ (see Kaltenegger et al. 2007). The corresponding biological surface fluxes required to sustain those mixing ratios are CH₄ = 1.01 × 10¹⁷ g yr⁻¹, N₂O = 3.14 × 10¹³ g yr⁻¹, and CH₃Cl = 9.06 × 10¹¹ g yr⁻¹. All other stellar types except the Sun use these surface fluxes as the boundary conditions for those gases. For H₂ and CO we used fixed deposition velocities

of 2.4 × 10⁻⁴ and 1.2 × 10⁻⁴ cm s⁻¹, respectively, corresponding to the maximum rate of transfer into an ocean (Domagal-Goldman et al. 2014). For the later stellar types, K7V, M1V, M3V, and the three observed MUSCLES stars, the CH₄ boundary condition was changed to a fixed mixing ratio (see also Segura et al. 2005; Rugheimer et al. 2014). For those stellar types, we used a mixing ratio of CH₄ corresponding to the last stable value, calculated for the K2V case, of 4.5 × 10⁻³. For the M8V model, we needed to further reduce the CH₄ mixing ratio to 4.0 × 10⁻³ for a stable atmosphere.

The third epoch corresponds to Earth as oxygen continues to rise at 0.8 Ga and the start of the proliferation of multicellular life. We model the atmosphere with a fixed mixing ratio of CO₂ = 0.01 and O₂ = 2.1 × 10⁻² (10% PAL) and a stellar flux of 94.8%. For the Earth–Sun case we fix the mixing ratios of the other biological gases to CH₄ = 1.65 × 10⁻³ (1000x PAL), N₂O = 9.15 × 10⁻⁸, and CH₃Cl = 5.0 × 10⁻¹⁰ (see Kaltenegger et al. 2007). The corresponding fluxes used for other stellar types are CH₄ = 2.75 × 10¹⁶ g yr⁻¹, N₂O = 2.08 × 10¹³ g yr⁻¹, and CH₃Cl = 7.76 × 10¹¹ g yr⁻¹. For H₂ and CO we used fixed deposition velocities as above. For the later stellar types, M3V, M8V, and the three observed MUSCLES stars, the CH₄ boundary condition was changed to a fixed mixing ratio. We used a mixing ratio of CH₄ corresponding to the last stable value, calculated for the M1V case, of 1.1 × 10⁻².

The fourth epoch corresponds to modern Earth. The model atmosphere has a fixed mixing ratio of CO₂ = 355 ppm and O₂ = 0.21. The biogenic fluxes were held fixed in the models in accordance with the fluxes that reproduce the modern mixing ratios in the Earth–Sun case. The surface fluxes for long-lived gases H₂, CH₄, N₂O, CO, and CH₃Cl were calculated such that the Earth around the Sun yields a $T_{\text{surf}} = 288$ K for surface mixing ratios: cH₂ = 5.5 × 10⁻⁷, cCH₄ = 1.6 × 10⁻⁶, cCO₂ = 3.5 × 10⁻⁴, cN₂O = 3.0 × 10⁻⁷, cCO = 9.0 × 10⁻⁸, and cCH₃Cl = 5.0 × 10⁻¹⁰ (see Rugheimer et al. 2013). The corresponding surface fluxes are -1.9 × 10¹² g H₂/year, 5.3 × 10¹⁴ g CH₄/year, 7.9 × 10¹² g N₂O/year, 1.8 × 10¹⁵ g CO/year, and 4.3 × 10¹² g CH₃Cl/year. M8V, CH₄, and N₂O were given a fixed mixing ratio of 1.0 × 10⁻³ and 1.5 × 10⁻², respectively (following Rugheimer et al. 2014).

3. RESULTS: UV FLUXES FOR PLANETS ORBITING FGKM STARS

For each model atmosphere and star type we calculate the UV flux reaching the surface of an Earth-like planet and compare that to the UV flux incident on the top-of-atmosphere (TOA). In Figure 1 we show the flux of the host star (black lines), the flux at the TOA (gray lines), and the flux reaching the ground for each epoch (colored lines) as seen from an observer at 10 pc. The flux from the host star relative to what is incident on the top of the atmosphere at 500 nm ranges from 10³ to 10¹⁰ for the M8V to F0V, respectively.

Figure 2 compares the incident (dashed) and surface (solid) flux at the planet at each of the four geological epochs for an F0V ($T_{\text{eff}} = 7000$ K), the Sun ($T_{\text{eff}} = 5778$ K), a K7V ($T_{\text{eff}} = 4250$ K), and an M8V star ($T_{\text{eff}} = 2300$ K) as a representation of the twelve stars modeled. For a pre-biotic atmosphere, the UV surface environment on planets orbiting any of the grid stars follow a similar trend with TOA flux levels being similar to surface flux levels for $\lambda > 200$ nm (see top left panel Figure 2). At 200 nm there is a sharp absorption in the

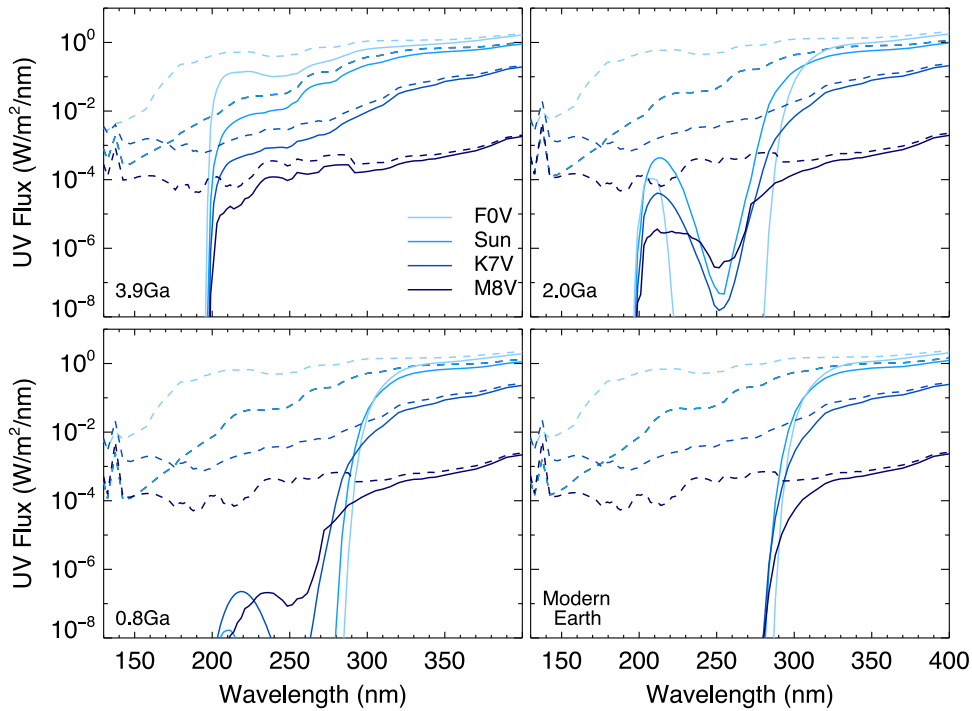


Figure 2. Incident stellar UV flux (dashed lines) and the surface UV flux (solid lines) at four geological epochs for a sample of four stellar types spanning the stellar effective temperature range for FGKM stars.

atmosphere by CO_2 and H_2O and no UV flux at wavelengths below 200 nm reaches the surface of the planet for any star type considered. With the rise of oxygen at 2.0 Ga to 1% PAL we see absorption of UV photons around 250 nm due to ozone (Figure 2, upper right). This is pronounced for F stars which have ozone column depths an order of magnitude higher at 2.0 Ga than G, K, and M stars due to higher incident UV flux and photolysis of O_2 producing O_3 (see Table 1 for O_3 column depths for all stars and epochs). As oxygen continues to rise at 0.8 Ga to 10% PAL and then to current levels for the modern Earth, absorption increases for $\lambda < 280$ nm due to ozone, effectively blocking UVC radiation from reaching the surface (see also Table 6).

Table 2 lists the TOA and surface UV fluxes for each stellar type and geological era for planets orbiting at the 1 AU equivalent distance for their host star. Tables 4–6 show the TOA and surface UV fluxes subdivided into UVA (315–400 nm), UVB (280–315 nm), and UVC (121.6–280 nm). Note that all fluxes have been diurnally averaged and calculated for a zenith angle of 60 degrees, representing a global average. We discuss the F0V–M8V results below and, comparable information for the three MUSCLES stars can be found in Table 2 and Tables 4–6.

At 3.9 Ga, 54%–77% of the total incoming stellar UV flux (121.6–400 nm) reaches the surface for a pre-biotic atmosphere orbiting different host stars. The lowest percentage of UV radiation reaches the ground for a pre-biotic Earth orbiting our M8V model star, and the highest percentage of UV radiation reaches the ground a K7V star (this trend holds for all epochs). Note that this does not correspond to the minimum and maximum of the absolute transmitted flux. The minimum UV flux that reaches the ground is 0.035 W m^{-2} for an M8V host star and the maximum is 61 W m^{-2} for an F0V host star in this epoch. However, the fraction of UVA, UVB, and UVC fluxes reaching the surface is different. In the UVA region, between 80% (G2V)–82% (M8V) of the incident flux and between

Table 1
Ozone Column Depths for the Grid of Host Stars (F0V to M8V)

Star	O_3 Column Depth			
	3.9 Ga	2.0 Ga	0.8 Ga	Modern Earth
F0V	1.76×10^{16}	5.13×10^{18}	9.07×10^{18}	1.15×10^{19}
F7V	3.93×10^{15}	2.20×10^{18}	6.17×10^{18}	8.62×10^{18}
Sun	1.84×10^{15}	6.01×10^{17}	4.23×10^{18}	5.29×10^{18}
G8V	4.21×10^{14}	1.73×10^{17}	1.62×10^{18}	5.56×10^{18}
K2V	7.32×10^{14}	1.23×10^{17}	1.08×10^{18}	3.62×10^{18}
K7V	1.10×10^{16}	5.31×10^{17}	7.38×10^{17}	3.46×10^{18}
M1V	1.01×10^{16}	5.37×10^{17}	7.37×10^{17}	4.03×10^{18}
M3V	9.88×10^{15}	3.97×10^{17}	5.66×10^{17}	3.59×10^{18}
M8V	1.43×10^{15}	2.63×10^{17}	3.15×10^{17}	2.47×10^{18}
GJ 581	6.76×10^{15}	3.55×10^{17}	4.75×10^{17}	1.18×10^{18}
GJ 832	2.49×10^{15}	3.46×10^{17}	6.25×10^{17}	1.59×10^{18}
GJ 1214	1.91×10^{16}	6.29×10^{17}	9.00×10^{17}	2.31×10^{18}

0.026 W m^{-2} (M8V) and 45 W m^{-2} (F0V) reaches the surface. In the UVB region, between 57% (F0V) and 59% (K2V) of the incident flux and between 0.0030 W m^{-2} (M8V) and 10 W m^{-2} (F0V) reaches the surface. In the UVC region between 15% (M1V) and 43% (G8V) of the incident flux and between $4.2 \times 10^{-3} \text{ W m}^{-2}$ (M8V) and 5.9 W m^{-2} (F0V) reaches the surface. The percentage and absolute flux reaching the ground depends on the interplay between the intensity of incoming UV radiation and the amount of ozone shielding.

At 2.0 Ga, 25% (M8V)–69% (K7V) of the total incoming stellar UV flux reaches the surface. In absolute flux, the minimum UV flux that reaches the surface is 0.032 W m^{-2} (M8V) and the maximum is 48 W m^{-2} (F0V). In the UVA region, between 73% (Sun)–78% (K7V) of the incident flux and between 0.029 W m^{-2} (M8V) and 47 W m^{-2} (F0V) reaches the surface for a planet. In

Table 2
Top-of-atmosphere (TOA) and Surface UV Fluxes for F, G, K, and M Stars

Star Type	UV fluxes 121.6 to 400 nm (W m^{-2})							
	3.9 Ga		2.0 Ga		0.8 Ga		Modern Earth	
	TOA	Surface	TOA	Surface	TOA	Surface	TOA	Surface
F0V	98.6	60.8	113.	48.1	123.	51.1	130.	53.3
F7V	62.6	44.2	71.7	39.1	78.1	40.8	82.4	42.5
Sun	37.9	28.1	43.6	27.8	51.4	30.4	55.0	32.3
G8V	31.3	23.4	35.8	23.8	39.0	24.4	41.2	25.0
K2V	16.5	12.6	19.0	13.1	20.7	13.8	21.8	14.2
K7V	4.79	3.71	5.68	3.94	6.19	4.29	6.53	4.50
M1V	2.00	1.22	3.39	1.19	3.69	1.30	3.89	1.36
M3V	0.934	0.510	1.75	0.465	1.91	0.503	2.01	0.533
M8V	0.0646	0.0347	0.125	0.0316	0.136	0.0349	0.144	0.0353
GJ 581	1.57	1.25	2.04	1.35	2.04	1.47	2.15	1.57
GJ 832	2.06	1.61	2.64	1.74	2.87	1.90	3.03	2.02
GJ 1214	0.943	0.722	1.19	0.778	1.19	0.847	1.25	0.902

Note. All fluxes have been diurnally averaged.

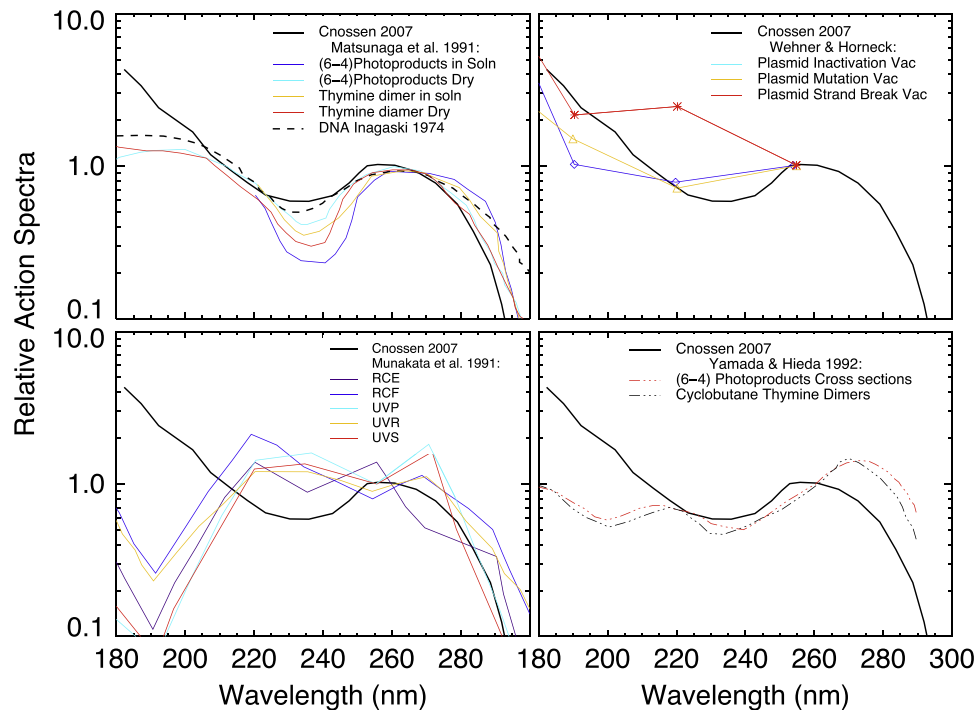


Figure 3. Action Spectra for photoproduct formation (top left, bottom right), DNA plasmid inactivation, mutation, and strand-breaks (top right), and the inactivation of bacterial spores (bottom left).

the UVB region, between 7.8% (F0V) and 48% (K2V) of the incident flux and between $2.2 \times 10^{-3} \text{ W m}^{-2}$ (M8V) and 2.5 W m^{-2} (G8V) reaches the surface. In the UVC region between $2.1 \times 10^{-3}\%$ (F0V) and 2.5% (G8V) of the incident flux and between $1.7 \times 10^{-4} \text{ W m}^{-2}$ (M8V) and $5.8 \times 10^{-4} \text{ W m}^{-2}$ (F0V) reaches the surface for a planet.

At 0.8 Ga, 26% (M8V)–69% (K7V) of the total incoming stellar UV flux reaches the surface. In absolute flux, the minimum UV flux that reaches the surface is 0.035 W m^{-2} (M8V) and the maximum is 51 W m^{-2} (F0V). In the UVA region, between 72% (F0V)–79% (M8V) of the incident flux and between 0.032 W m^{-2} (M8V) and 50 W m^{-2} (F0V) reaches the surface for a planet. In the UVB region, between 4.0% (F0V) and 36%

(M8V) of the incident flux and between $2.3 \times 10^{-3} \text{ W m}^{-2}$ (M8V) and 1.0 W m^{-2} (F7V) reaches the surface. In the UVC region between $1.3 \times 10^{-9}\%$ (F0V) and 0.097% (M8V) of the incident flux and between $4.1 \times 10^{-8} \text{ W m}^{-2}$ (F0V) and $1.4 \times 10^{-4} \text{ W m}^{-2}$ (M3V) reaches the surface for a planet.

For the modern Earth-like atmosphere, 25% (M8V)–69% (K7V) of the total incoming stellar UV flux reaches the surface. In absolute flux, the minimum UV flux that reaches the surface is 0.034 W m^{-2} (M8V) and the maximum is 53 W m^{-2} (F0V). In the UVA region, between 72% (F0V)–79% (M8V) of the incident flux and between 0.034 W m^{-2} (M8V) and 53 W m^{-2} (F0V) reaches the surface for a planet. In the UVB region, between 2.7% (F0V) and 17% (K7V) of the incident flux and

Table 3
Biologically Effective Irradiance E_{eff} , Relative to Modern Earth Levels

Star	Fluxes integrated from 182 to 370 nm							
	3.9 Ga		2.0 Ga		0.8 Ga		Modern Earth	
	E_{eff}	UV Ratio	E_{eff}	UV Ratio	E_{eff}	UV Ratio	E_{eff}	UV Ratio
F0V	3520	2.19	2.75	1.42	0.655	1.47	0.367	1.51
F7V	1680	1.57	10.8	1.23	1.13	1.23	0.524	1.27
Sun	611	0.969	41.3	0.906	1.53	0.942	1.00	1.00
G8V	482	0.806	107	0.797	7.71	0.781	0.678	0.773
K2V	181	0.416	56.5	0.425	5.93	0.433	0.671	0.436
K7V	26.2	0.102	1.95	0.105	1.28	0.114	0.105	0.117
M1V	44.5	0.0345	1.13	0.0301	0.662	0.0327	0.0317	0.0330
M3V	27.8	0.0150	1.26	0.0118	0.644	0.0126	0.0245	0.0126
M8V	2.33	0.00104	0.182	0.000807	0.132	0.000881	0.00393	0.000839
GJ 581	2.02	0.0312	0.432	0.0335	0.345	0.0364	0.120	0.0385
GJ 832	3.37	0.0403	0.616	0.0431	0.353	0.0468	0.105	0.0493
GJ 1214	2.67	0.0176	0.153	0.0186	0.0693	0.0202	0.0180	0.0213

between $9.9 \times 10^{-4} \text{ W m}^{-2}$ (M8V) and 0.80 W m^{-2} (Sun) reaches the surface. In the UVC region between $7.7 \times 10^{-29}\%$ (F0V) and $4.6 \times 10^{-9}\%$ (M8V) of the incident flux and between $2.5 \times 10^{-29} \text{ W m}^{-2}$ (F0V) and $4.3 \times 10^{-12} \text{ W m}^{-2}$ (M8V) reaches the surface for a planet.

To estimate the biologically relevant UV fluxes, it is useful to consider the damage to DNA and other biomolecules. An action spectrum is a parameter which gives the relative biological response effectiveness at different wavelengths. Multiplying the surface flux by the action spectrum gives the biologically effective irradiance. Integrated for a wavelength interval gives the biochemical effectiveness in that region, E_{eff} :

$$E_{\text{eff}} = \int_{\lambda_1}^{\lambda_2} F_{\text{surf}}(\lambda) S_{\lambda}(\lambda) d\lambda \quad (1)$$

where $F_{\text{surf}}(\lambda)$ is the surface flux ($\text{W m}^{-2} \text{ nm}^{-1}$) and $S_{\lambda}(\lambda)$ is the action spectrum of the biomolecule of interest in relative units. Action spectra are typically normalized at 260 or 300 nm and are given in relative units. The damage of such molecules as the thymine dimers and (6-4)photoproducts correspond to DNA damage and have similar action spectra (see Figure 3 and Matsunaga et al. 1991). We use a DNA action spectrum for $182 \text{ nm} < \lambda < 370 \text{ nm}$ based on Cnossen et al. (2007) for $\lambda < 260 \text{ nm}$ and Setlow (1974)⁸ for $\lambda > 265 \text{ nm}$. For comparison to other shortwave action spectra ($\lambda < 300$) we plot the response curves for DNA photoproducts formation (Matsunaga et al. 1991; Yamada & Hieda 1992), DNA plasmid inactivation, mutation, and strand-breaks (Wehner & Horneck 1995), and the inactivation of bacterial spores (Munakata et al. 1991; see Figure 3). The action spectra agree to within an order of magnitude and is shown to 360 nm in Figure 5.

We normalized our DNA action spectrum at 260 nm and reference to modern Earth-Sun when quoting the biologically effective irradiance as given in Equation (2) to estimate the

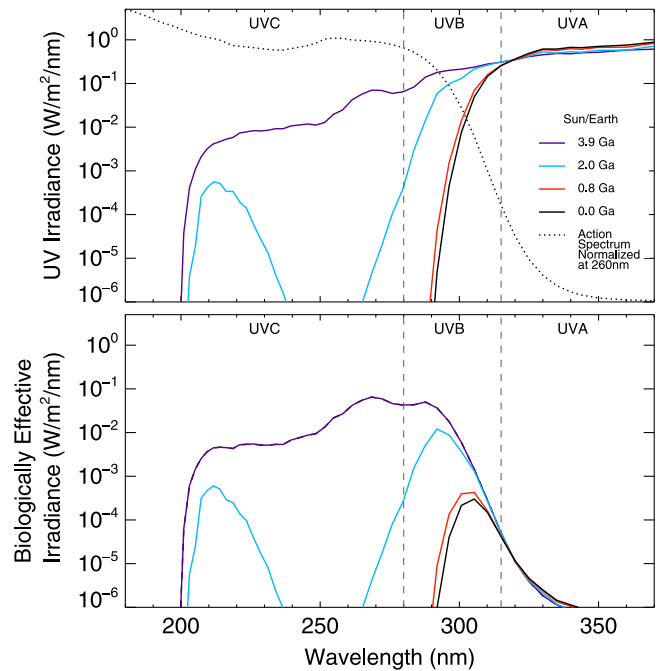


Figure 4. UV fluxes at the surface for the Earth-Sun case through time with the dashed line as the DNA Damage Action Spectrum (top). The relative biological effectiveness of UV damage is the convolution of the flux and action spectrum over wavelength (bottom).

damage through geological time.

$$E_{\text{eff}} = \frac{\int_{182 \text{ nm}}^{370 \text{ nm}} F_{\text{surf}}(\lambda) S_{\lambda \text{ DNA}}(\lambda) d\lambda}{\int_{182 \text{ nm}}^{370 \text{ nm}} F_{\text{surf modern}}(\lambda) S_{\lambda \text{ DNA}}(\lambda) d\lambda} \quad (2)$$

Table 3 gives the biologically effective irradiance and the absolute UV flux ratio compared to the modern Earth-Sun model for each geological epoch and stellar type.

Because biological damage is heavily focused in the UVC and UVB regions (shown in Figure 4) the E_{eff} values are much higher for the early-Earth case than is intuitive from the absolute fluxes, especially around F-type host stars. For an F0V prebiotic atmosphere, we calculate $E_{\text{eff}} = 3520$, three orders of magnitude larger than for modern Earth and 6 times larger than

⁸ From database: <http://www.esrl.noaa.gov/gmd/grad/antuv/docs/version2/descVersion2Database3.html>.

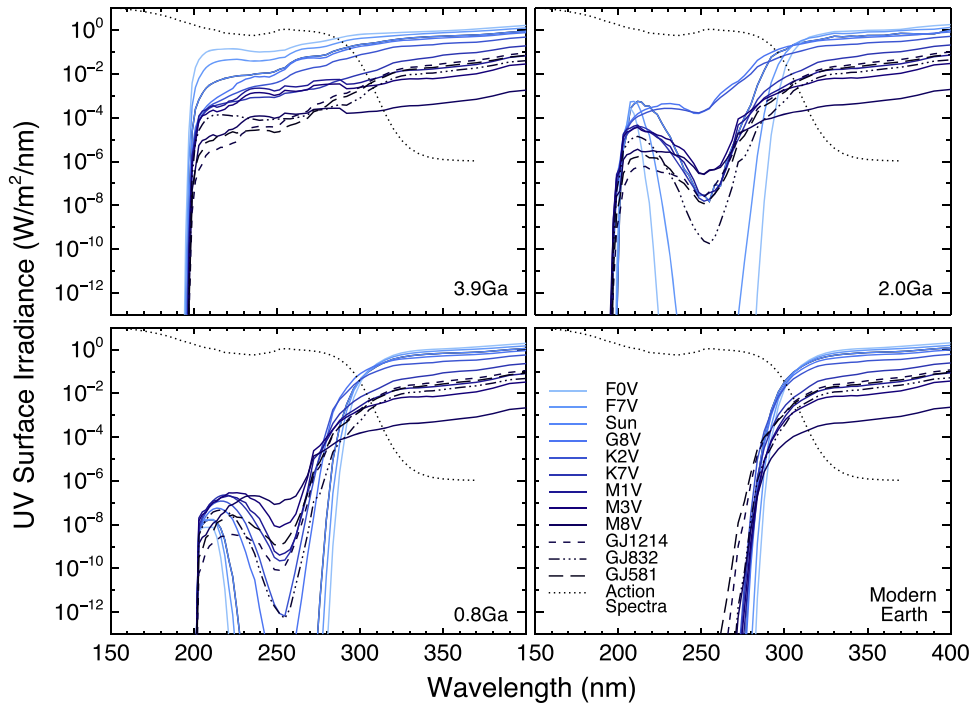


Figure 5. Surface UV flux levels ($\text{W m}^{-2} \text{nm}^{-1}$) for an Earth-sized planet at four geological epochs orbiting F0V to M8V host stars. Lines have been smoothed for clarity. DNA action spectrum is shown as a dotted line.

Table 4
Top-of-atmosphere (TOA) and Surface UVA fluxes for F, G, K, and M Stars

Star Type	UVA fluxes 315 to 400 nm (W m^{-2})							
	3.9 Ga		2.0 Ga		0.8 Ga		Modern Earth	
	TOA	Surface	TOA	Surface	TOA	Surface	TOA	Surface
F0V	56.0	44.7	64.1	46.5	69.8	50.2	73.6	52.7
F7V	43.8	34.9	50.2	37.0	54.7	39.8	57.7	41.8
Sun	29.9	23.8	34.4	25.6	40.2	29.5	43.1	31.5
G8V	25.0	19.9	28.6	21.3	31.1	23.0	32.8	24.4
K2V	13.9	11.1	15.9	12.0	17.4	13.0	18.3	13.8
K7V	4.31	3.51	4.94	3.83	5.38	4.18	5.68	4.45
M1V	1.30	1.06	1.49	1.14	1.62	1.25	1.71	1.34
M3V	0.505	0.412	0.578	0.435	0.630	0.475	0.664	0.521
M8V	0.0331	0.0260	0.0379	0.0292	0.0412	0.0324	0.0435	0.0343
GJ 581	1.48	1.21	1.70	1.32	1.85	1.44	1.95	1.54
GJ 832	1.91	1.56	2.19	1.70	2.38	1.86	2.51	1.98
GJ 1214	0.858	0.700	0.983	0.764	1.07	0.832	1.13	0.890

Note. All fluxes have been diurnally averaged.

the early Earth–Sun model. This E_{eff} value is 1600 times larger than the ratio of UV fluxes at the surface for a prebiotic world orbiting an F0V host star, which highlights the importance of including the action spectrum when considering biological effects. For the anoxic atmosphere at 3.9 Ga, all stars have E_{eff} larger than one, the modern Earth–Sun value. We find the smallest E_{eff} values are about 2 times the modern Earth–Sun value in our model for the surface of a prebiotic planet orbiting GJ 581. It has 31 times less total UV ground radiation and 300 times less biologically effective radiation as the prebiotic Earth–Sun model.

At the rise of oxygen at 2.0 Ga (1% PAL O_2), we see a substantial reduction in E_{eff} values. The surface of planets

orbiting F, G, and K grid stars still receive UV radiation corresponding to E_{eff} values higher than modern Earth–Sun, but planets orbiting M stars receive biologically effective irradiances near or less than modern Earth. At 0.8 Ga (10% PAL O_2), we see further reduction in E_{eff} values. For modern Earth’s atmosphere composition, the surface of planets orbiting all other host stars receive UV fluxes that correspond to E_{eff} values less than one. For the F stars, this is due to increased shielding from higher abundances of ozone. For the cooler K and M stars, this is due to a lower abundance of stellar UV photons incident on the atmosphere.

In Figure 4 we show the action spectrum (normalized at 260 nm, dashed line) with the Earth–Sun UV surface fluxes

Table 5
Top-of-atmosphere (TOA) and Surface UVB Fluxes for F, G, K, and M Stars

Star Type	UVB fluxes 280 to 315 nm (W m^{-2})							
	3.9 Ga		2.0 Ga		0.8 Ga		Modern Earth	
	TOA	Surface	TOA	Surface	TOA	Surface	TOA	Surface
F0V	18.0	10.3	20.6	1.60	22.5	0.905	23.7	0.644
F7V	11.4	6.67	13.1	2.13	14.2	0.998	15.0	0.692
Sun	5.77	3.41	6.76	2.19	8.04	0.902	8.63	0.798
G8V	4.71	2.79	5.39	2.45	5.87	1.31	6.19	0.583
K2V	2.00	1.19	2.29	1.10	2.49	0.714	2.63	0.404
K7V	0.261	0.153	0.145	0.110	0.325	0.108	0.343	0.0566
M1V	0.126	0.0730	0.0844	0.0466	0.158	0.0461	0.266	0.0219
M3V	0.0737	0.0422	0.00590	0.0281	0.0920	0.0275	0.0970	0.0120
M8V	0.00516	0.00298	0.0863	0.00219	0.00643	0.00230	0.00678	0.000986
GJ 581	0.0578	0.0350	0.0721	0.0310	0.0721	0.0321	0.0760	0.0280
GJ 832	0.0754	0.0457	0.0863	0.0399	0.0941	0.0389	0.0992	0.0322
GJ 1214	0.0279	0.0169	0.0319	0.0141	0.0348	0.0143	0.0367	0.0116

Note. All fluxes have been diurnally averaged.

Table 6
Top-of-atmosphere (TOA) and Surface UVC Fluxes for F, G, K, and M Stars

Star Type	UVC fluxes 121.6 to 280 nm (W m^{-2})							
	3.9 Ga		2.0 Ga		0.8 Ga		Modern Earth	
	TOA	Surface	TOA	Surface	TOA	Surface	TOA	Surface
F0V	24.7	5.89×10^0	28.4	5.83×10^{-4}	30.9	4.08×10^{-8}	32.6	2.50×10^{-29}
F7V	7.46	2.64×10^0	8.57	2.00×10^{-3}	9.34	9.42×10^{-8}	9.86	1.63×10^{-23}
Sun	2.20	8.71×10^{-1}	2.63	4.03×10^{-3}	3.20	9.31×10^{-8}	3.38	2.30×10^{-16}
G8V	1.59	6.86×10^{-1}	1.84	4.58×10^{-2}	2.01	5.58×10^{-7}	2.12	3.96×10^{-17}
K2V	0.589	2.46×10^{-1}	0.709	3.48×10^{-2}	0.773	7.79×10^{-6}	0.814	4.17×10^{-13}
K7V	0.209	3.99×10^{-2}	0.441	3.88×10^{-4}	0.480	1.39×10^{-5}	0.506	1.14×10^{-13}
M1V	0.549	7.97×10^{-2}	1.73	6.14×10^{-4}	1.88	5.79×10^{-5}	1.99	4.57×10^{-15}
M3V	0.342	4.98×10^{-2}	1.07	8.55×10^{-4}	1.17	1.39×10^{-4}	1.23	3.38×10^{-14}
M8V	0.0254	4.22×10^{-3}	0.0802	1.72×10^{-4}	0.0874	8.49×10^{-5}	0.0921	4.27×10^{-12}
GJ 581	0.0253	2.03×10^{-3}	0.110	6.25×10^{-5}	0.119	1.75×10^{-5}	0.126	6.87×10^{-8}
GJ 832	0.0706	3.77×10^{-3}	0.360	9.99×10^{-5}	0.392	1.01×10^{-5}	0.414	6.08×10^{-9}
GJ 1214	0.0559	4.63×10^{-3}	0.0742	1.00×10^{-4}	0.0808	1.00×10^{-6}	0.0853	1.15×10^{-11}

Note. All fluxes have been diurnally averaged.

through the four geological epochs. Note the strong overlap for the pre-biotic atmosphere. Already at 2.0 Ga most of the UV flux has been attenuated by O_3 in the atmosphere, causing a sharp decrease in the E_{eff} values for the later epochs. The bottom panel of Figure 4 shows the surface UV flux weighted by the DNA action spectrum, highlighting which wavelengths and epochs have the most damaging irradiation for molecules with similar responses as the DNA action curve.

Despite harsh UVB and UVC radiation conditions present on a planet without an ozone shield, certainly prebiotic chemistry and the origin of life flourished on the early Earth. Being under a layer of water or rock would mitigate the problems induced by high UV fluxes. Microbial mats scatter light such that the lower levels have only 1% of incident light at 0.5 mm depth, and subsurface community hosting layers of sandstone reduce light levels to 0.005% of incidence (Nienow & Friedmann 1993; Garcia-Pichel et al. 1994; Nienow et al. 1988; Cockell 1999). As well, prebiotic organic polymers and dissolved inorganic ions may provide sufficient protection from UV degradation in as little as 2 mm of ocean water (Cleaves & Miller 1998).

Figure 5 shows the smoothed lines for the surface UV flux for an Earth-sized planet at the four geological epochs with the action spectrum curve overlaid for all grid stars modeled.

4. DISCUSSION AND CONCLUSIONS

In this study, we investigated the exoplanet surface UV fluxes for Earth-like planets orbiting a grid of F, G, K, and M stars at four possible biogeological epochs in the evolution of life. We use the input flux from 12 different stellar types, 9 model stars in the FGKM range with $T_{\text{eff}} = 4250 \text{ K}$ to $T_{\text{eff}} = 7000 \text{ K}$, and three M stars (GJ 581, GJ 832, and GJ 1214) with observed UV fluxes for our calculations. The atmospheres selected correspond to a pre-biotic Earth model at 3.9 Ga, a model atmosphere for the early rise of oxygen at 2.0 Ga and 0.8 Ga, and modern Earth biology. We also consider the amount of UVA, UVB, and UVC fluxes, with the latter two showing the greatest changes among stellar types and geological epochs. For a pre-biotic atmosphere, a significant portion of incident UVC flux reaches the surface. Whereas in the modern atmosphere for planets orbiting any grid star, all

UVC photons are effectively shielded by ozone. For all epochs, the smallest percentage of total UV flux compared to incident flux reaching the ground is for an M8V star and the highest fraction is for a K7V star due to the balance of available near- and far-UV photons and the amounts of ozone produced. However in terms of absolute flux, the smallest amount reaches the surface is for an M8V host star and the largest amount for an F0V star.

To analyze the potential biological consequences of the UV surface environment for the origin and evolution of life, we convolve the UV surface fluxes with the DNA action spectrum as a proxy for biological damage. While it is uncertain whether DNA will arise as the primary information carrier on another planet, current biosignature searches are focused on finding carbon-based chemistry. Since the action spectra for other carbon based biomolecules follow similar trends in their actions spectra, we use DNA as a proxy for biochemical effectiveness of UV radiation damage. The surface of pre-biotic worlds have significantly higher E_{eff} values than around the early Sun. *Deinococcus radiodurans* is one of the most radiation tolerant organism known, withstanding 1000x the lethal human radiation dose. UV tolerance experiments show *D. radiodurans* can survive 400 J m^{-2} of 254 nm radiation without significant loss of viability with appreciable loss of viability occurring around $500\text{--}600 \text{ J m}^{-2}$ (Gascón et al. 1995).

A layer of water or soil might be needed to shield life for hot stars. Even for a planet orbiting the least UV active star in our grid, the biologically effective irradiance on the surface of a pre-biotic world is several times the value for modern Earth. With higher ozone concentration in the atmosphere, that value decreases for planets orbiting all star types.

We model clear sky atmospheres for all planets at all epochs which on average will represent an upper limit to the UV radiation environment at the surface since clouds most frequently block up to 80% of incoming UV radiation (Grant & Heisler 1997; Parisi & Downs 2004). However clouds also can focus more UV radiation to the ground depending on cloud cover and type, increasing the amount of UV radiation reaching the surface. Earth measurements of UVA and UVB radiation on cloudy versus cloud-free days show clouds can enhance UV radiation by a factor of 1.08 and 1.4 for UVA and UVB radiation, respectively (Parisi & Downs 2004).

Note that higher CO_2 and CH_4 concentrations in the atmosphere as well as hazes could further protect the surface from UV radiation (Cnossen et al. 2007; Cockell 1999). In addition, UV photons may also positively contribute to pre-biotic reactions leading to the origin of life (Senanayake & Idriss 2006; Barks et al. 2010; Ritson & Sutherland 2012; Patel et al. 2015).

Our models provide boundary conditions for the UV environment on the surface of Earth-like planets orbiting a grid of FGKM stars from pre-biotic to modern Earth atmosphere. Our results inform photo biological assessments, pre-biotic chemistry, and early life evolution experiments.

We find that a pre-biotic Earth (3.9 Gyr ago) orbiting an F0V star receives 6 times the biologically effective radiation as around the early Sun and 3500 times the modern Earth-Sun levels. A pre-biotic Earth orbiting an M8V star receives around 300 times less biologically effective radiation and 2 times modern Earth-Sun levels.

For the second geological epoch with 1% PAL O_2 , a planet orbiting an F0V and M8V star receives 15 and 230 times less

biologically effective radiation than the Earth-Sun model at that geological epoch, respectively. For the third geological epoch with 10% PAL O_2 , a planet orbiting an F0V and M8V star receives 2 and 12 times less biologically effective radiation than the Earth-Sun model at that geological epoch, respectively. For the fourth geological epoch, corresponding to modern Earth concentrations of O_2 , a planet orbiting an F0V and M8V star receives 3 and 250 times less biologically effective radiation than the modern Earth-Sun, respectively. Note that for all epochs after oxygen begins to rise in the atmosphere, both the hottest stars and coolest stars have less biologically effective radiation. For the hottest stars, this is due to increased ozone shielding from higher-UV environments, and for the coolest stars this is due to less absolute UV flux.

We would like to thank Kevin France for discussions concerning the MUSCLES database and Sukrit Ranjan for discussions concerning DNA action spectra. This work has made use of the MUSCLES M dwarf UV radiation field database. We would also like to acknowledge support from DFG funding ENP KA 3142/1-1 and the Simons Foundation (290357, Kaltenecker and 290360, Sasselov).

REFERENCES

- Allard, F. 2014, in Proc. Int. Astronomical Union 8 (Cambridge: Cambridge Univ. Press), 271
- Allard, F., Hauschildt, P. H., & Schwenke, D. 2000, *ApJ*, **540**, 1005
- Barks, H. L., Buckley, R., Grieves, G. A., et al. 2010, *ChemBioChem*, **11**, 1240
- Batalha, N. M., Rowe, J. F., Bryson, S. T., et al. 2013, *ApJS*, **204**, 24
- Beichman, C., Lawson, P., Lay, O., et al. 2006, Proc. SPIE, **6268**, 62680S
- Beichman, C. A., Woolf, N. J., & Lindensmith, C. A. 1999, in The Terrestrial Planet Finder (TPF): a NASA Origins Program to search for habitable planets (Pasadena, CA: JPL Publications)
- Borucki, W. J., Agol, E., Fressin, F., et al. 2013, *Sci*, **340**, 587
- Borucki, W. J., Koch, D. G., Basri, G., et al. 2011, *ApJ*, **736**, 19
- Cash, W. 2006, *Natur*, **442**, 51
- Claire, M. W., Sheets, J., Cohen, M., et al. 2012, *ApJ*, **757**, 95
- Cleaves, H. J., & Miller, S. L. 1998, *PNAS*, **95**, 7260
- Cnossen, I., Sanz-Forcada, J., Favata, F., et al. 2007, *JGRE*, **112**, E02008
- Cockell, C. S. 1998, *Journal of Theoretical Biology*, **193**, 717
- Cockell, C. S. 1999, *Icar*, **141**, 399
- Cockell, C. S. 2000, *P&SS*, **48**, 203
- Domagal-Goldman, S. D., Segura, A., Claire, M. W., Robinson, T. D., & Meadows, V. S. 2014, *ApJ*, **792**, 90
- France, K., Froning, C. S., Linsky, J. L., et al. 2013, *ApJ*, **763**, 149
- Garcia-Pichel, F., Mechling, M., & Castenholz, R. W. 1994, *Applied and Environmental Microbiology*, **60**, 1500
- Gascón, J., Oubiña, A., Pérez-Lezaun, A., & Urmeneta, J. 1995, *Current Microbiology*, **30**, 177
- Grant, R. H., & Heisler, G. M. 1997, *JApMe*, **36**, 1336
- Haqq-Misra, J. D., Domagal-Goldman, S. D., Kasting, P. J., & Kasting, J. F. 2008, *AsBio*, **8**, 1127
- Kaltenecker, L., Fridlund, M., & Karlsson, A. 2006, *Ap&SS*, **306**, 147
- Kaltenecker, L., & Sasselov, D. 2011, *ApJ*, **736**, L25
- Kaltenecker, L., Sasselov, D., & Rugheimer, S. 2013, *ApJ*, **775**, L47
- Kaltenecker, L., Traub, W. A., & Jucks, K. W. 2007, *ApJ*, **658**, 598
- Kasting, J. F., & Ackerman, T. P. 1986, *Sci*, **234**, 1383
- Kasting, J. F., Holland, H. D., & Pinto, J. P. 1985, *JGR*, **90**, 10497
- Kasting, J. F., Pollack, J. B., & Crisp, D. 1984, *JAtC*, **1**, 403
- Kerwin, B. A., & Remmele, R. L. 2007, *Journal of Pharmaceutical Sciences*, **96**, 1468
- Kharcha, P., Kasting, J. F., & Siefert, J. 2005, *Geobiology*, **3**, 53
- Kurucz, R. L. 1979, *ApJS*, **40**, 1
- Marty, B., Zimmermann, L., Pujol, M., Burgess, R., & Philippot, P. 2013, *Sci*, **342**, 101
- Matsunaga, T., Hieda, K., & Nikaido, O. 1991, *Photochemistry and Photobiology*, **54**, 403
- Munakata, N., Saito, M., & Hieda, K. 1991, *Photochemistry and Photobiology*, **54**, 761

- Nienow, J. A., & Friedmann, E. I. 1993, in *Antarctic Microbiology*, ed. E. I. Friedmann (New York: Wiley), 343
- Nienow, J. A., McKay, C. P., & Friedmann, E. I. 1988, *MicEc*, 16, 271
- Parisi, A. V., & Downs, N. 2004, *Photochemical and Photobiological Sciences*, 3, 643
- Patel, B. H., Percivalle, C., Ritson, D. J., Duffy, C. D., & Sutherland, J. D. 2015, *NatCh*, 7, 301
- Pavlov, A. A., Brown, L. L., & Kasting, J. F. 2001, *JGR*, 106, 23267
- Pavlov, A. A., & Kasting, J. F. 2002, *AsBio*, 2, 27
- Pavlov, A. A., Kasting, J. F., Brown, L. L., Rages, K. A., & Freedman, R. 2000, *JGR*, 105, 11981
- Quintana, E. V., Barclay, T., Raymond, S. N., et al. 2014, *Sci*, 344, 277
- Ritson, D., & Sutherland, J. D. 2012, *NatCh*, 4, 895
- Rugheimer, S., Kaltenegger, L., Segura, A., Linsky, J. L., & Mohanty, S. 2015, *ApJ*, in press
- Rugheimer, S., Kaltenegger, L., Zsom, A., Segura, A., & Sasselov, D. 2013, *AsBio*, 13, 251
- Sato, S., Cuntz, M., Guerra Olvera, C. M., Jack, D., & Schröder, K.-P. 2014, *IJAsB*, 13, 244
- Seager, S., & Bains, W. 2015, *Science Advances*, 1, e1500047
- Segura, A., Kasting, J. F., Meadows, V., et al. 2005, *AsBio*, 5, 706
- Segura, A., Krelove, K., Kasting, J. F., et al. 2003, *AsBio*, 3, 689
- Segura, A., Meadows, V. S., Kasting, J. F., Crisp, D., & Cohen, M. 2007, *A&A*, 472, 665
- Segura, A., Walkowicz, L. M., Meadows, V., Kasting, J., & Hawley, S. 2010, *AsBio*, 10, 751
- Senanayake, S. D., & Idriss, H. 2006, *PNAS*, 103, 1194
- Setlow, R. B. 1974, *PNAS*, 71, 3363
- Som, S., Catling, D. C., Hammeijer, J., Polivka, P., & Buick, R. 2012, *Natur*, 484, 359
- Tevini, M. (ed.) 1993, in *UV-B Radiation and Ozone Depletion: Effects on Humans, Animals, Plants, Microorganisms, and Materials* (Boca Raton, Florida: Lewis Publishers)
- Toon, O. B., McKay, C. P., Ackerman, T. P., & Santhanam, K. 1989, *JGR*, 94, 16287
- Traub, W. A., Levine, M., Shaklan, S., et al. 2006, *Proc. SPIE*, 6268, 62680T
- Udry, S., Bonfils, X., Delfosse, X., et al. 2007, *A&A*, 469, L43
- Voet, D., Gratzner, W., Cox, R., & Doty, P. 1963, *Biopolymers*, 1, 193
- Wehner, J., & Horneck, G. 1995, *Journal of Photochemistry and Photobiology B: Biology*, 28, 77
- Yamada, H., & Hieda, K. 1992, *Photochemistry and Photobiology*, 55, 541